Spin waves in the spin-flop phase of $RbMnF_3$

1994 J. Phys.: Condens. Matter 6 10341

(http://iopscience.iop.org/0953-8984/6/47/017)

J. Phys.: Condens. Matter 6 (1994) 10341–10355. Printed in the UK

Spin waves in the spin-flop phase of $RbMnF_3$

D A Tennant†, D F McMorrow†§, S E Nagler†‖, R A Cowley† and B Fåk‡¶
† Oxford Physics, Clarendon Laboratory, Parks Road, Oxford OX1 3PU, UK
‡ Institut Laue–Langevin, Grenoble, France

Received 1 September 1994

Abstract. The spin-wave excitations of the near-ideal 3D Heisenberg antiferromagnet $RbMnF_3$ have been measured in the presence of an applied field using neutron scattering. Detailed measurements of both the wave vector and field dependence of the excitations were made for fields up to 5.7 T. For applied fields $\geqslant 0.26$ T, the spins undergo a spin-flop transition. In this phase the twofold degeneracy of the zero-field spin waves is lifted. A rigorous analysis of the data, allowing for the effects of instrumental resolution, shows that the excitations are well explained by linear spin-wave theory. No evidence is found for higher-order processes, such as have been found in systems of lower dimensionality.

1. Introduction

$RbMnF_3$ is probably the closest realization of an isotropic, 3D Heisenberg antiferromagnet (AF) [1]. It has a cubic perovskite structure with a lattice spacing of $a = 4.218$ Å [1]. The orbital moment of each manganese ion is quenched by the cubic crystal field and it carries a spin-only moment of quantum number $S = 5/2$. Windsor and Stevenson [2] have made measurements of the dispersion of the magnons in $RbMnF_3$ in zero field using neutron scattering. They were able to explain their results using a linear spin-wave theory with an isotropic exchange constant J of 0.29 ± 0.03 meV between nearest neighbours, and a second-neighbour constant of less than 0.02 meV. In fact the next-nearest-neighbour exchange strengths in perovskite fluorites are normally only of the order of 1% of the nearest-neighbour exchange value [3]. Antiferromagnetic resonance (AFMR) measurements give a magnetic anisotropy field of only 4.5 Oe [4] and [5], which is only some 6×10^{-6} that of the exchange field. The low value of the anisotropy field can be explained in that the Mn^{2+} cation has no orbital moment and there is no dipolar interaction because of the cubic symmetry of the site. The magnetic moments order at temperatures below the Néel ordering temperature, $T_N = 83$ K, and in this phase the spins align antiferromagnetically along the [1, 1, 1] crystallographic easy directions [4] and [5]. The structure of $RbMnF_3$ and the four magnetic easy axes are illustrated in figure 1.

When a uniform magnetic field greater than 0.26 T is applied along the ordering direction of the system [6], [1, 1, 1] direction say, in the 3D Néel ordered phase, a spin-flop transition occurs. This transition field is lower for non-easy-axis directions. In this phase the Mn^{2+} moments align antiferromagnetically and almost perpendicular to the field but slightly canted out of the plane in the direction of the field to minimize their Zeeman energy. In the absence

§ Present address: Risø National Laboratory, DK-4000, Roskilde, Denmark.
‖ Permanent address: Department of Physics, University of Florida, Gainesville, FL 32611, USA.
¶ Present address: CENG, Grenoble, France.

0953-8984/94/4710341+15$19.50

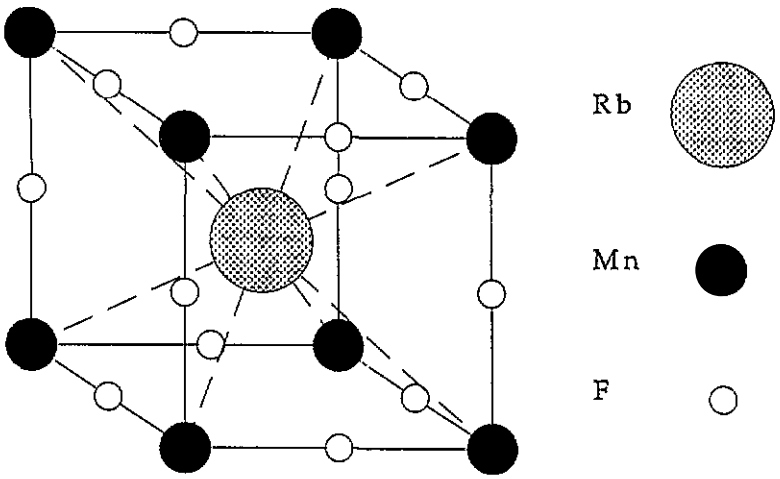

Figure 1. The crystal structure of $RbMnF_3$. The magnetic easy axes are indicated by the dotted lines.

of a magnetic field the spin waves are twofold degenerate, and Windsor and Stevenson [2] were able to observe a single magnon branch only. The application of a field breaks the rotational symmetry of the modes, which precess around the ordering direction perpendicular to the field, and the dispersion of the low-energy spin waves is expected to split into two branches. The spin-wave dynamics of a 3D Heisenberg AF in such a spin-flop phase has not previously been measured. In the analogous one-dimensional systems [7] two-magnon processes give rise to additional modes, and there is evidence that this may also occur in two-dimensional systems [8]. Such excited modes are a consequence of zero-point spin fluctuations which are largely supposed in the 3D case. The aim of our experiment was to measure the wavevector and field dependence of the splitting between the magnon branches in $RbMnF_3$, and to compare our measurements with the predictions of linear spin-wave theory.

The paper is organized in the following way. After outlining the relevant theory in section 2, we continue by presenting our experimental method in section 3. In section 4 the results and analysis are given.

2. Antiferromagnetic spin waves in an applied field

In this section the excitations and field-induced transitions between the ordered phases of a 3D Heisenberg AF in an applied field are considered in more detail. Figure 2 is a generalized phase diagram of this system for the case where a magnetic field is applied along an anisotropy direction [9]. The ordered system, which consists of a simple cubic lattice of Mn sites, can be subdivided into two interpenetrating body-centred cubic sublattices denoted by A and B. In the Néel (AF) phase the spins on the A sublattice align along the $(+z)$-direction, where z is an anisotropy direction, and those on the B sublattice point in the $(-z)$-direction. For simplicity the case where the magnetic field is applied down a unique anisotropy direction is considered first. The Hamiltonian for this system can then be written as

$$\hat{H}_{\mathrm{AF}} = 2J \sum_{l,m} \boldsymbol{S}_l \cdot \boldsymbol{S}_m - g\mu_{\mathrm{B}} B \sum_l S_l^z - g\mu_{\mathrm{B}} B_{\mathrm{an}} \left(\sum_l S_l^z - \sum_m S_m^z \right) \qquad (1)$$

where l counts over sublattice A and m is over sublattice B, B is the magnitude of the applied field, B_{an} is an alternating anisotropy field and J is the exchange energy which takes a non-zero value for nearest neighbours only. The calculation of the excitation energies for this Hamiltonian is straightforward using a standard linear spin-wave approach and is derived in many places (see, for example, [10] and [11]).

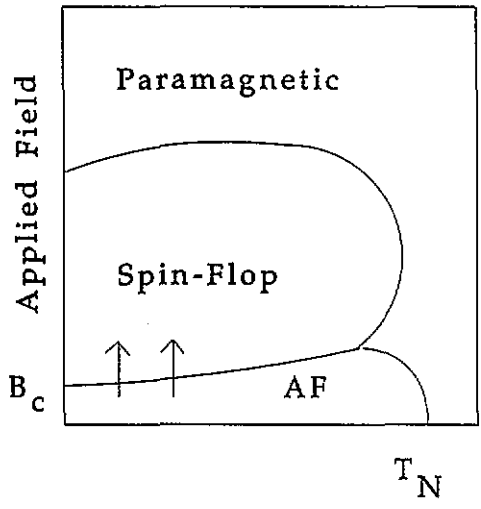

Figure 2. A schematic phase diagram for a uniaxial antiferromagnet in an applied magnetic field. The antiferromagnetic–spin-flop transition is indicated by arrows.

The dispersion of the spin-wave excitations consists of two magnon branches which are split by the field and are given by

$$\omega_k^{\pm} = \left[\left(\omega_E + \omega_A\right)^2 - \gamma_k^2 \omega_E^2\right]^{1/2} \pm \omega_H \tag{2}$$

where $\omega_E = 2zSJ/\hbar$, $\omega_A = g\mu_B B_{an}/\hbar$ and $\omega_H = g\mu_B B/\hbar$. The term

$$\gamma_k = \frac{1}{z}\sum_{\delta} e^{ik\cdot\delta}$$

is the sum over the z nearest-neighbour vectors δ. In zero field the two spin-wave branches, defined in equation (2), are degenerate. As the strength of the applied field B is increased from zero, the upper and lower branches move upwards and downwards in energy, respectively. The lower-branch frequency of equation (2) becomes negative and therefore unstable for applied fields B that satisfy the condition

$$B > B_c^u = B_{an}\sqrt{\left(1 + \frac{2\omega_E}{\omega_A}\right)}. \tag{3}$$

Thus for applied fields greater than the critical field B_c^u a spin-flop transition is induced and the system enters a spin-flop phase, where the spins then lie almost perpendicular to the field direction. Figure 2 shows the transition boundary between the spin-flop and AF phases as a function of both applied field B and temperature T, as calculated by Anderson and Callen [12] using temperature renormalization of the spin-wave energies. The applied transition fields between the spin-flop and AF phases for a uniaxial system exhibit hysteresis, and the transition is first order in nature.

2.1. Spin-flop excitations

In the spin-flop phase the spins cant out of the x–y plane by a small angle φ. The torques induced on a spin by the applied field and exchange balance for an angle φ that satisfies the relation $\sin(\varphi) = \omega_H/(2\omega_E + \omega_A)$ [13]. The calculation of the spin-wave frequencies in the spin-flop phase has been carried out by Wang and Callen [13] for the uniaxial Hamiltonian. (In their analysis Wang and Callen include an extra term $\xi = (1-(2S)^{-1})^{1/2}$ to account for quantum corrections to the low-lying spin states. As this correction is small for large spin S it is not included in any of the results quoted here.) The spin-wave frequencies are split by the field into two branches, and the dispersion of the modes as a function of the wave vector $\boldsymbol{k}$ is given by

$$\omega_k^{\pm} = \omega_E\left[1 \pm \gamma_k\right]^{1/2}\left[1 \pm \gamma_k \cos(2\varphi) - \left(\omega_A/\omega_E\right)\cos^2(\varphi)\right]^{1/2}. \tag{4}$$

For small values of k the lower branch is almost linear in k because of the first square root and it goes to zero at $k = 0$. The upper mode has an energy gap at $k = 0$ which decreases as the applied field strength $\boldsymbol{B}$ is decreased. The spin-flop phase becomes unstable for negative spin-wave energies and this occurs for fields B lower than a critical field,

$$B < B_c^l = B_{an}\left(\frac{2\omega_E}{\omega_A} - 1\right)\left(\frac{\omega_A}{2\omega_E + \omega_A}\right)^{1/2} \tag{5}$$

below which a transition from the spin-flop to the AF phase occurs. The field B_c^l is lower than B_c^u and so there is a hysteresis in the applied transition field between the two ordered phases. The magnitude of the hysteresis depends on the relative magnitudes of exchange and anisotropy fields and in the case where $\omega_E \gg \omega_A$ the two critical fields B_c^l and B_c^u converge to the same value, given by $B_{an}(2\omega_E/\omega_A)^{1/2}$. Antiferromagnetic resonance measurements of the transition fields in the 3D uniaxial AF compounds MnF_2 and $MnBr_2{\cdot}4H_2O$ [14] have established such hysteresis effects and the measured critical fields agree with the values calculated using equations (3) and (5). We note that the anisotropy of $RbMnF_3$ is very much smaller than that of MnF_2 and $MnBr_2{\cdot}4H_2O$, and in addition $RbMnF_3$ has four easy axes, rather than uniaxial anisotropy, which complicates the measurements somewhat. However, measurements of the critical field have been made for a field applied down the ordering direction [6], and this value agrees with the value of 0.26 T calculated from the known exchange and anisotropy parameters.

In the case where $\boldsymbol{B}$ is applied down the $[1,-1,0]$ direction of $RbMnF_3$, the geometry used in our experiment, both the $[1,1,1]$ and $[1,1,-1]$ easy directions are perpendicular to the applied field and the spins are found to lie almost perpendicular to the $[1,-1,0]$ direction for all $\boldsymbol{B}$ [6]. Consequently no AF–spin-flop transition is expected to be observed for $RbMnF_3$ for a field applied along $[1,-1,0]$.

The modification of the analysis of Wang and Callen [13] for the uniaxial Hamiltonian to take account of an in-plane anisotropy in the spin-flop phase is straightforward. Such a case occurs for the magnetic field applied down $[1,-1,0]$. The anisotropy field in the ordered phase will be directed along each spin direction in the spin-flop phase with the field in the z-direction of the Hamiltonian, equation (1), becoming zero. As each magnon is a deviation of $\Delta S^z = \pm 1$, the in-plane anisotropy contribution to each sublattice is then given by $\omega_A a_k^{+} a_k$ and $\omega_A b_k^{+} b_k$, respectively, where a_k and b_k are the usual sublattice spin-wave operators. The result of this term in the excitation spectrum can be seen by inspection of

equations (11) and (21) in the paper of Wang and Callen [13]. Making a simple substitution into equation (7), where the out-of-plane anisotropy is taken as zero, gives the dispersion

$$\omega_k^{\pm} = \omega_E\left(1 \mp \gamma_k + \frac{\omega_A}{\omega_E}\right)^{1/2}\left(1 \pm \gamma_k \cos(2\varphi) + \frac{\omega_A}{\omega_E}\right)^{1/2} \tag{6}$$

where ω_A is now the frequency of the in-plane anisotropy as defined above in equation (2). In zero field the spin waves are identical to those of the uniaxial AF, and in the case where the anisotropy contribution ω_A is zero they are identical to the result for the spin-flop excitations.

2.2. *Neutron scattering cross sections*

The one-magnon scattering cross sections of unpolarized neutrons have been calculated by Lovesey [15] for the spin-flop phase. The case where no staggered field is applied, $B_{an} = 0$, was considered, which is a reasonable approximation for $RbMnF_3$. The cross section for a scattering process in which the neutron loses energy $\hbar\omega$ and wave-vector transfer $\boldsymbol{Q}$ can be written in terms of the spin–spin correlations, and for the case of spin-only scattering as applies to $RbMnF_3$, the dynamical cross-section is

$$S(\boldsymbol{Q}, \omega) = \frac{1}{2\pi N}\int_{-\infty}^{\infty} \mathrm{d}t\ \mathrm{e}^{\mathrm{i}\omega t}\sum_{l,m}\mathrm{e}^{\mathrm{i}\boldsymbol{Q}\cdot(\boldsymbol{R}_l - \boldsymbol{R}_m)}\sum_{\alpha,\beta}\left(\delta_{\alpha\beta} - \hat{Q}_\alpha\hat{Q}_\beta\right)\left\langle S_l^\alpha(0)S_m^\beta(t)\right\rangle \tag{7}$$

where α and β denote Cartesian components. Lovesey in [15] has calculated the spin–spin correlations and his results of relevance to the argument are quoted here. For convenience a function $Z_f(\omega)$ is defined in [15] to simplify the resulting expressions, such that

$$Z_f(\omega) = \left(n_f + 1\right)\delta\left(\omega - \omega_f\right) + n_f\,\delta\left(\omega + \omega_f\right) \tag{8}$$

where the labels $f = 1$ and 2 denote the lower and upper branches respectively, and $n_f = (\exp(-\omega_f/k_BT) - 1)^{-1}$ is the usual Bose occupation function. By defining $p_1 = 1$ and $p_2 = -1$, the structure factors for the spin-wave excitations are given by the expressions

$$\begin{aligned} X_f = {} & \left(1 + p_f\gamma_k\sin^2(\varphi)\right)\left(1 + \sin^2(\varphi)\hat{Q}_z^2 + \cos^2(\varphi)\hat{Q}_y^2\right) \\ & + p_f\gamma_k\cos^2(\varphi)\left(1 - \left(1 + \cos^2(\varphi)\hat{Q}_z^2 - \left(1 + \sin^2(\varphi)\right)\hat{Q}_y^2\right)\right. \end{aligned} \tag{9}$$

and

$$\begin{aligned} Y_f = {} & \cos^2(\varphi)\left\{\left(1 - p_f\gamma_k\right)\hat{Q}_y^2 - \left(1 + p_f\gamma_k\right)\right\} + \sin^2(\varphi)\left\{\left(1 + p_f\gamma_k\right)\left(1 + p_f\gamma_k\right)\left(1 + \hat{Q}_z^2\right)\right\} \\ & + \left(1 + \cos(2\varphi)\right)\hat{Q}_z^2 \end{aligned} \tag{10}$$

where the spins lie in the y–z plane. Using this notation the scattering cross-section derived by Lovesey for a mode at reduced wave vector $\boldsymbol{k}$ is then given by

$$S(\boldsymbol{Q}, \omega) = \frac{1}{2N}\left|\sum_m \mathrm{e}^{\mathrm{i}\boldsymbol{R}_m\cdot(\boldsymbol{Q}+\boldsymbol{k})}\right|^2\sum_f\left(\frac{Z_f(\omega)}{\omega}\right)\left(X_f + p_f\cos(\boldsymbol{\delta}\cdot\boldsymbol{\tau})Y_f\right) \tag{11}$$

where the sum over the sublattice m is non-zero only when $\boldsymbol{Q} + \boldsymbol{k} = \boldsymbol{\tau}$ is a reciprocal lattice vector of the sublattice. At small wave vectors $\boldsymbol{k}$ away from $\boldsymbol{\tau}$ the spin waves exhibit

the usual $(1/\omega)$ structure factor associated with antiferromagnets. The case of interest to this discussion is that of scattering near a superlattice peak ($\cos(\delta \cdot \tau) = -1$) and for small applied fields ($\sin \varphi \ll 1$). The spins are then almost aligned along the y-direction. The lower spin-wave branch corresponds to the in-plane component (IPC) and has correlations in the plane along the x-direction, whereas the upper mode is the out-of-plane component (OPC) and the spin correlations from this mode are perpendicular to the plane, in the z-direction. Neutrons measure the spin components perpendicular to the wave vector transfer Q, and so for a scattering vector in the spin-flop plane the intensity of the OPC will be independent of the actual direction of those spins within the plane. However, the intensity of the IPC does depend on this direction, and consequently has a lower overall intensity factor. The dynamical cross-section for the inelastic scattering of unpolarized neutrons is approximated by the simple expression

$$S(Q, \omega) \approx A\frac{|k|}{|k'|}\frac{1}{\omega}\big(A_1 Z_1(\omega) + A_2 Z_2(\omega)\big) \tag{12}$$

where $A_1 = (1 - \hat{Q}_x^2)$ and $A_2 = (1 - \hat{Q}_z^2)$, A is a scale factor, and $Z_1(\omega)$ and $Z_2(\omega)$ corresponding to the lower and upper branches, equation (8).

3. Experimental details

The measurements were performed on the IN12 triple-axis spectrometer at the Institut Laue–Langevin, in Grenoble, France. The pre-sample monochromation of the neutron beam is provided by a variable-curvature pyrolytic graphite (PG) (002) monochromator and the energy of the scattered beam analysed using the (002) reflection from a flat PG crystal. The sample was a large single crystal (5 cm^3) of $RbMnF_3$. It was mounted in the vertical-field cryomagnet with the $[1, -1, 0]$ axis vertical so as to allow access to the $(-\frac{1}{2}, -\frac{1}{2}, \frac{1}{2})$ reciprocal-lattice point. The $[1, -1, 0]$ scattering plane of $RbMnF_3$ is shown in figure 3. The instrument collimation was chosen at 33′–30′–30′–30′ giving an in-plane wave vector resolution measured at 0.01 Å full width at half maximum (FWHM) and an energy width of 0.03 meV (FWHM). Measurements were performed with the wave vector of the incident neutrons being held fixed and the spectrometer in the focused (W) configuration. The k_i-values used in the experiment were between 1.25 $Å^{-1}$ and 1.40 $Å^{-1}$ and a cooled beryllium filter was inserted before the sample to reduce contamination from higher-order components of the beam. The sample temperature was maintained at a constant $T = 4.3$ K throughout the experiment. Measurements of the splitting of the spin-wave branches were made in magnetic fields from 0–5.68 T. Scans in both neutron energy loss and gain were performed for each field at a series of neutron wave vector transfers Q directed along the $[-1, -1, 1]$ direction, with these measurements being made around the antiferromagnetic reciprocal-lattice point $(-\frac{1}{2}, -\frac{1}{2}, \frac{1}{2})$ as indicated in figure 3.

4. Results and analysis

In an applied field of $B = 5.68$ T a constant-Q scan at an antiferromagnetic zone centre $\tau_M = (-\frac{1}{2}, -\frac{1}{2}, -\frac{1}{2})$ revealed an excitation at 0.6 meV, shown in figure 4, in addition to a strong quasi-elastic component. The excitation frequency of the upper mode decreases with field; in zero field this excitation was found to be absent. When scans were performed

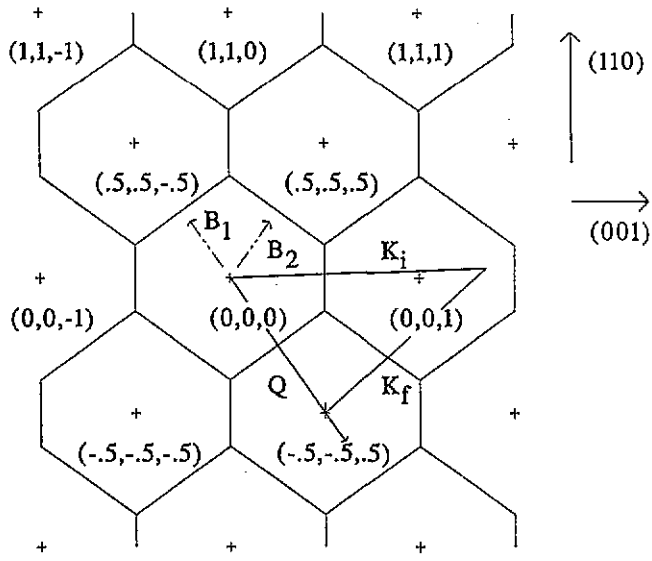

Figure 3. The $[1, 1, -1]$ scattering plane of $RbMnF_3$. A typical scattering triangle is shown in solid lines, and the anisotropy directions B_1 and B_2 are shown as dashed lines.

away from the zone centre, two modes were clearly resolved for wave vector transfers $Q = \tau_M + k$, for $k = (-\zeta, -\zeta, \zeta)$ and $0 < \zeta < 0.020$, with the second, lower mode emerging from the quasi-elastic scattering. Figure 5 displays an example of one such scan in energy, and was taken at $\zeta = 0.007$. At wave vectors $\zeta > 0.020$ the two modes merged and could no longer be resolved.

One striking feature of the line shapes of the excitations shown in figures 4 and 5 is that they are strongly asymmetric in energy. This could be caused by instrumental resolution or else some other process such as an intrinsic broadening in energy of the spin-wave modes. Taking full account of the instrumental effects in the analysis allows the theoretical cross-section to be checked, including details of the line shapes if required.

4.1. Resolution effects

Before describing in detail our method of fitting the data we first consider in qualitative terms how the asymmetric line shapes might be explained by resolution effects. Figure 6 shows a representative resolution ellipsoid and simple dispersion surface of a low-lying magnon mode. It is clear from the figure that as the ellipsoid scans in energy, the elongation of the ellipsoid out of the scattering plane gives rise to a tail at higher energies in the scattering profile. Such an elongation is characteristic of the vertical divergence of the beam.

The intensity of scattered neutrons $I(Q, \omega)$ at an energy ω and wave vector Q is determined by convoluting the spin-wave cross-section $S(Q, \omega)$ over the resolution volume. We start by defining a set of Cartesian coordinates such that the wave vector transfer Q is directed along the x-direction, the transverse direction in the scattering plane is directed along y, and the out-of-plane direction is along z. The predicted intensity is found by evaluating the four-dimensional integral

$$I(Q, \omega) = \frac{A_f}{\sigma_\omega \sigma_x \sigma_y \sigma_z} \int_{-\infty}^{\infty} d\omega' \exp\left(-\frac{(\omega - \omega')^2}{2\sigma_\omega^2}\right)$$

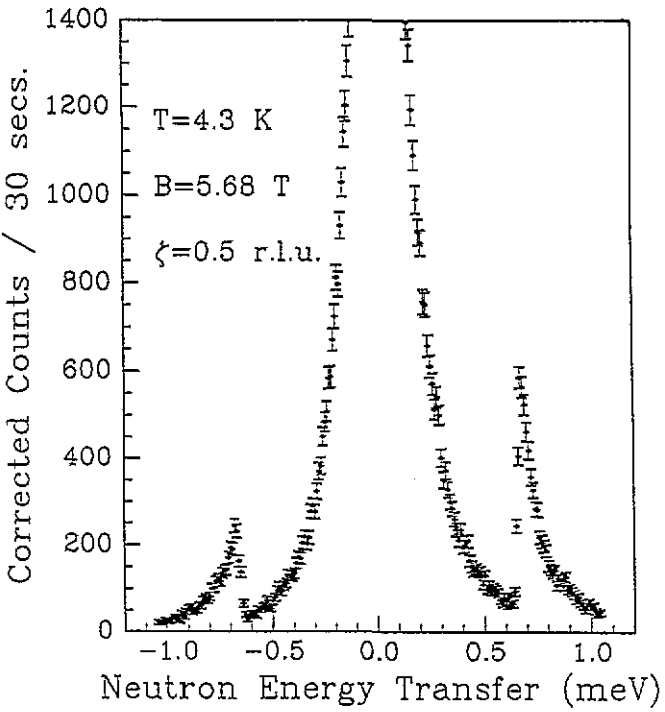

Figure 4. The scattered neutron intensity for a scan of the neutron energy transfer with Q held fixed at the magnetic zone centre $\tau_M = (-\frac{1}{2}, -\frac{1}{2}, \frac{1}{2})$.

$$\times \int\int\int_{-\infty}^{\infty} \mathrm{d}^3q \exp\left(-\frac{(q_x - Q)^2}{2\sigma_x^2} - \frac{q_y^2}{2\sigma_y^2} - \frac{q^2}{2\sigma_z^2}\right)$$

$$\times \frac{1}{|\omega|}\left[(n_\omega + 1)\,\delta(\omega' - \omega_f(q_x, q_y, q_z)) + n_\omega\,\delta(\omega' + \omega_f(q_x, q_y, q_z))\right] \tag{13}$$

where σ_x, σ_y, σ_z and σ_ω are the dimensions of the ellipsoid in wave vector and energy respectively. The pole in the δ-function for the lower ($f = 1$) and upper ($f = 2$) mode is given by the dispersion $\omega_f(Q)$, equation (6). Unfortunately the numerical evaluation of the 4D convolution is computationally inefficient. We need to introduce suitable approximations in order to obtain an expression suitable for a least-squares analysis.

The expression given in equation (13) may be simplified somewhat. First we note that the component of the ellipsoid along the y-direction is tangential to the energy contours of the dispersion surface at the point Q, as is the out-of-plane component (along the z-direction). The out-of-plane component is dominant and the integral over q_y can safely be ignored at wave vector transfers away from the zone centre. At wave vector transfers close to the zone centre this in-plane component is included as a small geometric correction to q_x. Further, if the reduced wave vector transfers k are small and the dispersion, equation (6), can be simplified, then $\omega_f(k) = \omega_E(Q^2 + \omega_f(0)^2/\omega_E^2)^{1/2}$, where $\omega_f(0)$ is the energy gap at the zone centre and k is the wave vector away from the zone centre. Integrating over the vertical component, q_z gives the simplified expression

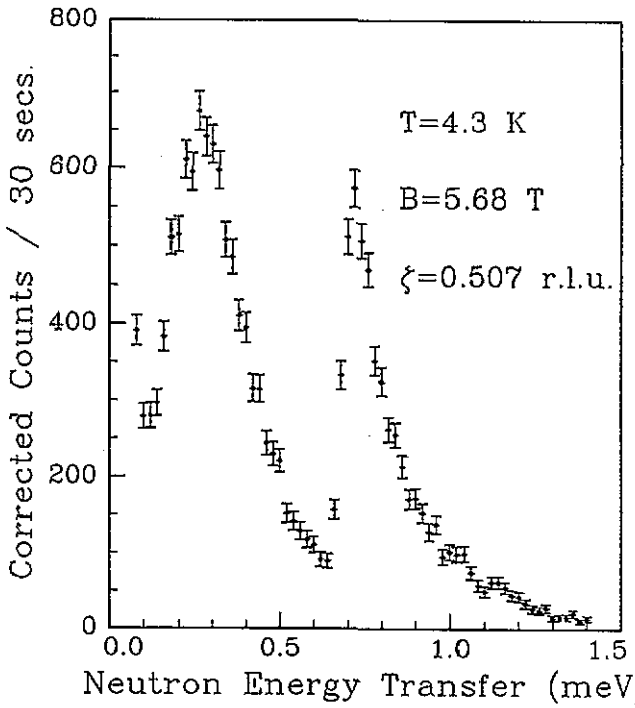

Figure 5. The scattered neutron intensity for a scan of the neutron energy transfer with Q held fixed at a wave-vector away from the zone centre.

$$I(\boldsymbol{Q}, \omega) = |F(\boldsymbol{Q})|^2 A_f \int_{-\infty}^{\infty} \mathrm{d}q_x \ \exp\left(\frac{(q_x - Q)^2}{2\sigma_x^2}\right) \int_{-\infty}^{\infty} \mathrm{d}\omega' \ N_{\omega'}(T) \times \exp\left(\frac{(\omega' - \omega)^2}{2\sigma_\omega^2}\right)\left[\frac{\exp(q_z^2/2\sigma_z^2)}{q_z(\omega')}\right] \tag{14}$$

where the $N_{\omega'}(T)$ are the Bose–Einstein occupation factor $n_\omega + 1$ and n_ω, for ω positive and negative respectively, and $q_z = [(\omega^2 - \omega^2(0))/\omega_E^2 - q_x^2]^{1/2}$. Note that the integration over the variable ω' has a square-root singularity at $\omega = (\omega^2(0) + (\omega_E q_x)^2)^{1/2}$. This integration can be evaluated on a computer if an open-ended integration routine such as the Romberg method [16] is used. The integration over q_x was also evaluated numerically.

4.2. Comparison with measurements

As the measurements were made in the fixed-incident-energy configuration of the spectrometer, the data have been corrected for the variation in resolution volume with the final wave vector k_{final} [17]. The data are corrected by dividing each point by the factor $k_{\text{final}}^3 \cot \varphi_A$ where φ_A is the analyser Bragg angle. The corrected data are then proportional to the scattering cross-section $S(\boldsymbol{Q}, \omega)$ and so can be modelled by a calculation of the double integral in equation (14). A least-squares method [16] was used to fit the exchange and anisotropy parameters of the Hamiltonian to data. The initial resolution parameters were determined for the scan using the computer program RESCAL. A fit to the zone-centre scan in a field of 5.68 T gave an energy gap of 0.655 meV. By comparing scattering data on the energy gain side with that on the loss side the temperature was fixed at a value of

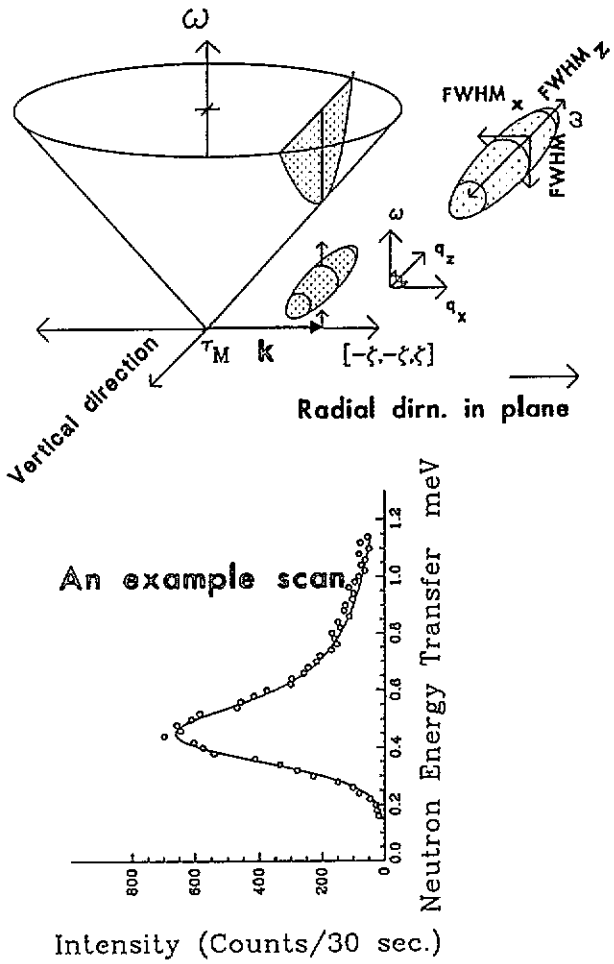

Figure 6. A diagrammatic representation of a constant-Q scan. The resolution ellipsoid is shown passing through the dispersion.

$T = 4.3$ K. Scans further out in ζ are more sensitive to the exchange energy J, and fitting to these gave a value of 0.32±0.025 meV which is in agreement with the value of Windsor and Stevenson (0.29±0.03 meV) [2].

By varying the vertical resolution width in the fits, a value of 0.08 $Å^{-1}$ was able to fit all scans at each wave vector and applied field B consistently. An example fit to a zone-centre scan is shown as the solid line in figure 7, this fit has a normalized $\chi^2 \sim 1$. To investigate the importance of the vertical resolution a zone-centre scan was also performed in a field of 5.68 T using a *de*focused monochromator. Presumably the flat monochromator has a smaller vertical divergence of the neutron beam. When the resolution was again allowed to vary, the width in this case was found to be 0.06 $Å^{-1}$ as compared with that calculated using the computer program RESCAL (0.04 $Å^{-1}$). A possible reason for the discrepancy in calculated width is that a Gaussian resolution profile for the vertical divergence was assumed. If the actual profile is trapezoidal then the effective vertical resolution is increased.

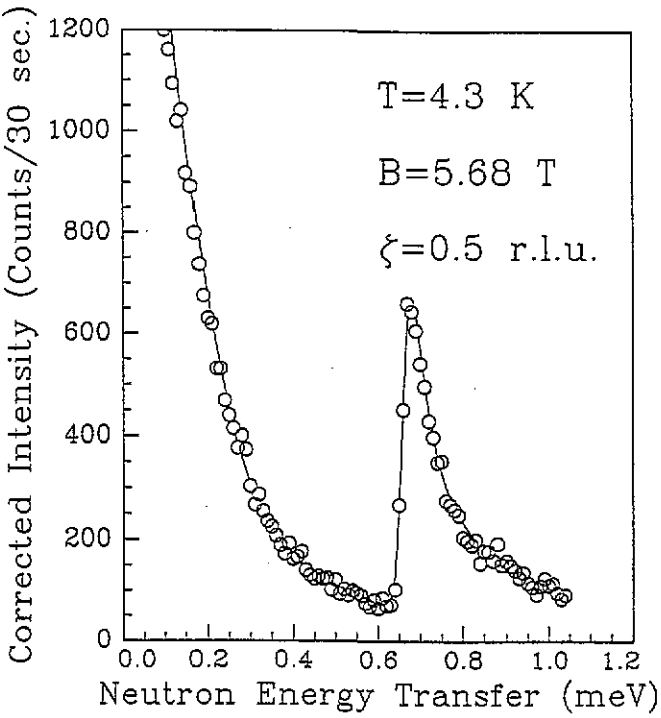

Figure 7. The solid line is a fit as described in the text to the linear spin-wave theory.

Calculations using such simple profiles are in line with this interpretation. To account for the vertical resolution with any more certainty would require measurements of the out-of-plane resolution profile. Another possible mechanism for the line broadening induced by the magnetic field has been suggested in [16]. However, the broadening would be expected to be symmetric and the effect is expected to be small at fields of 6 T in $RbMnF_3$. Thus we conclude that the asymmetry is presumably due to the resolution of the instrument.

Our measurements also give the relative intensities of the two modes. For each applied field the intensity factors A_1 and A_2 of the lower (A_1) and upper (A_2) modes were also fitted, equation (12). For an applied field $\boldsymbol{B}$ of magnitude 5.68 T they were found to be $A_1/A_2 = 0.502 \pm 0.001$. If the spins order into two equivalent domains directed along the anisotropy directions $[1, 1, 1]$ and $[1, 1, -1]$ indicated in figure 3, then the ratio would be 0.55. However, polarized neutron measurements by Cox *et al* [18] of the domain structure in an applied field $\boldsymbol{B}$ of magnitude 1.0 T directed along the $[1, 1, -2]$ direction showed that the spins ordered in a random domain structure within the plane rather than poling into a single domain along the uniquely perpendicular $[1, 1, 1]$ easy direction. A random domain structure would give a ratio of intensities between lower and upper modes of exactly 0.5, which agrees with the measured value. It is noteworthy that the applied field 5.68 T is considerably greater than the small anisotropy fields (4.5 G) along the $[1, 1, 1]$ and $[1, 1, -1]$ directions and should therefore dominate the ordering process.

Figure 8 shows the line shapes calculated using the parameters obtained above, for the scans made in an applied field $\boldsymbol{B}$ of magnitude 5.68 T at a series of wave vectors ζ. The scattering computed on the basis of the fitted parameters provides an excellent description

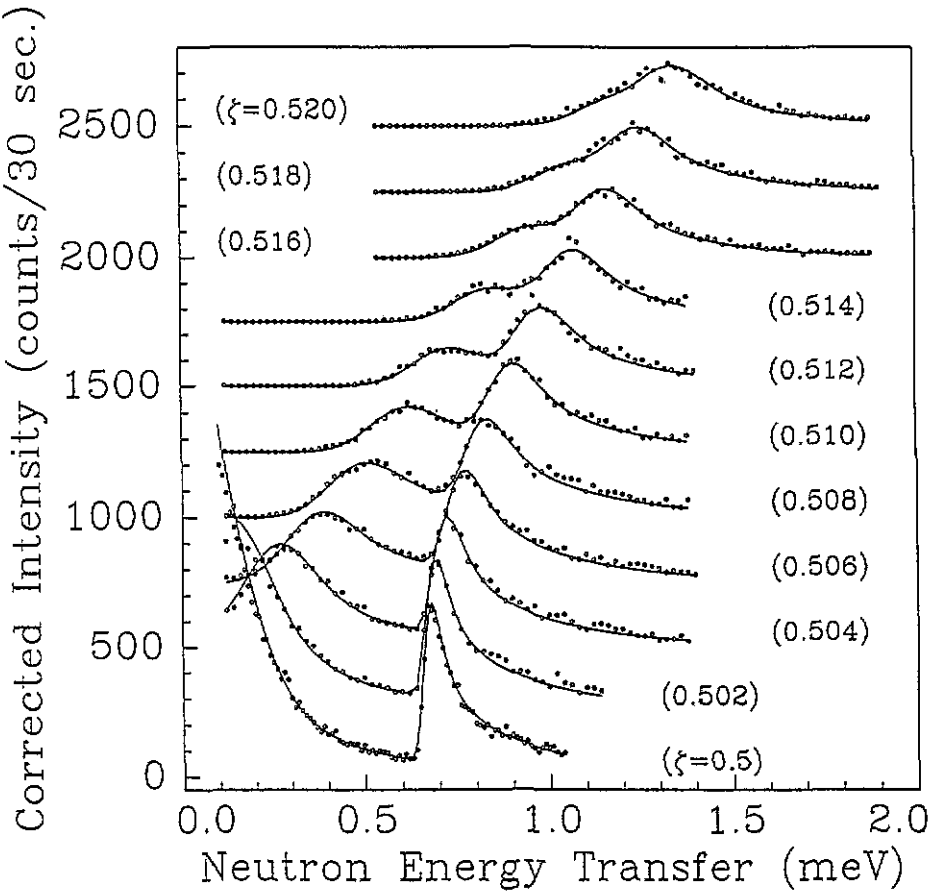

Figure 8. Constant-Q scans measured in an applied field of 5.68 T. The solid lines are calculated line shapes as described in the text.

of all the scans. The dispersion for this field given by equation (6) is shown in figure 9. The region $0.50 < \zeta < 0.52$, which has been covered by these scans, is shown as an inset on the plot. Figure 10 shows the calculated line shapes for a zero-field scan, and again uses the same exchange and resolution parameters as figure 5. A small zone-centre anisotropy gap of 0.05 ± 0.02 meV was introduced for the zero-field fit, and this has been included in the calculation of the line shape shown in figure 10.

The field dependence of the zone-centre frequency as determined from measurements with applied fields $\boldsymbol{B}$ with magnitudes between zero and 5.68 T is shown in figure 11. The frequencies have been determined using least-squares fitting as outlined above and the results are plotted in figure 11. Also shown in figure 11 are the predicted field behaviours of the gap energy in three different circumstances. The dotted line indicates the zone-centre energy gap of the upper modes where the field $\boldsymbol{B}$ is applied down a unique anisotropy axis, equation (4), and it shows the expected spin-flop–AF transition at 0.26 T. The dashed line is the energy gap for the case where the anisotropy field $\boldsymbol{B}_{an}$ is zero. And the solid line is the frequency calculated for an anisotropy field $\boldsymbol{B}_{an}$ perpendicular to the applied

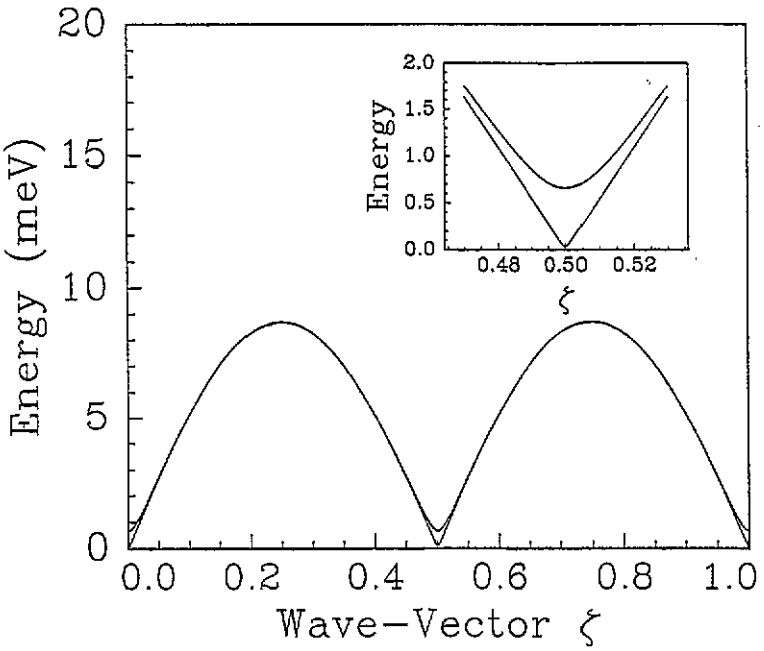

Figure 9. The spin-wave dispersion of $RbMnF_3$ in an applied magnetic field of 5.68 T. The inset shows the dispersion close to the zone centre.

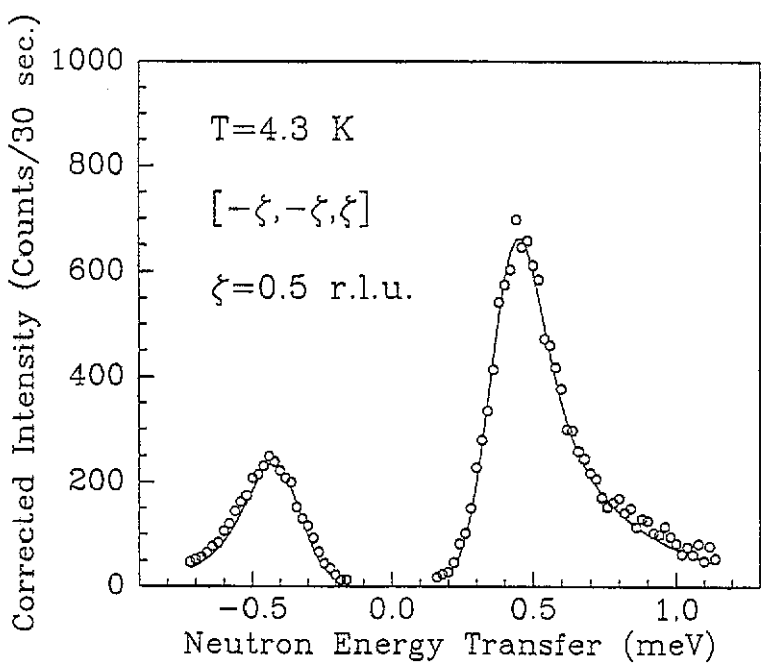

Figure 10. A typical constant-Q scan measured in zero magnetic field. No splitting of modes is seen.

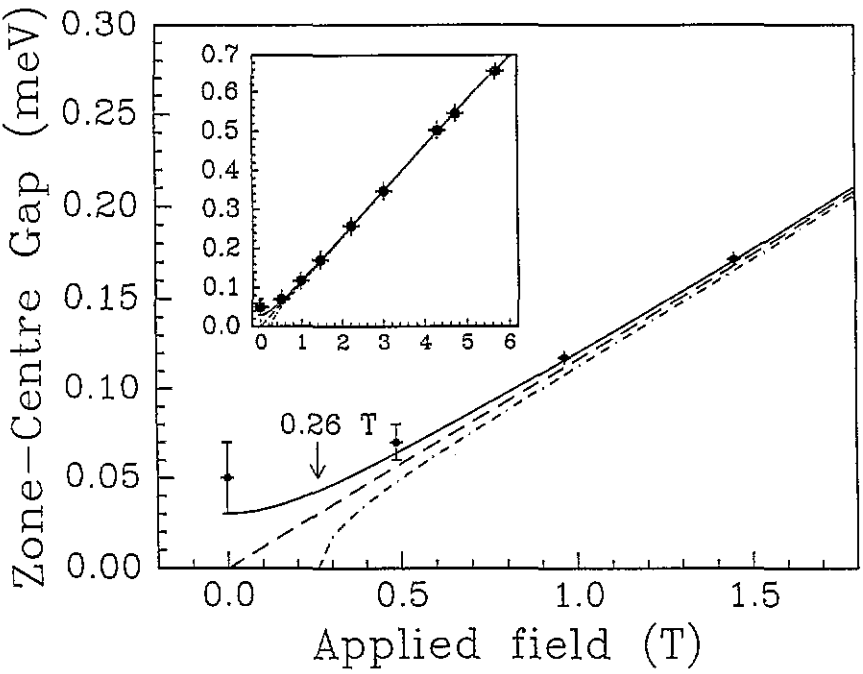

Figure 11. The variation of the zone-centre energy gap as a function of applied magnetic field. The solid, dashed and dotted lines are from spin-wave calculations as described in the text.

field, equation (6), which is the case here, where B has been applied along $[1,-1,0]$. The anisotropy energy determined from AFMR measurements of 4.5 Oe, [4] and [5], was used for these calculations. The measured frequencies are seen to be well accounted for by linear spin-wave theory.

5. Summary

The excitations in the spin-flop phase of $RbMnF_3$ have been studied using the IN12 neutron triple-axis spectrometer. The magnetic field was applied down the $[1,-1,0]$ direction. Constant-Q scans around the $(-\frac{1}{2}, -\frac{1}{2}, \frac{1}{2})$ reciprocal-lattice point show strongly asymmetric line shapes which were found to be the result of a poor vertical resolution. Taking this into account the line shapes of the measurements at all applied fields and wave vectors can be fitted consistently using linear spin-wave theory which also considers the in-plane anisotropy fields. The exchange constant determined is in good agreement with that obtained from other studies. No evidence of extra modes, such as occur in one- and two-dimensional systems, was observed.

Acknowledgments

We would like to thank CENG, Grenoble, France for providing the superconducting magnet. We also wish to thank the SERC for funding the experiment and providing Alan Tennant with a studentship. SEN has been funded by the US DOE and a grant from the NSF.

References

[1] de Jongh L J and Miedema A R 1974 *Adv. Phys.* **23** 1
[2] Windsor C G and Stevenson R W H 1966 *Proc. Phys. Soc.* **87** 501
[3] Yamaguchi Y and Sakamoto N 1969 *J. Phys. Soc. Japan* **27** 1444
Pickart S J, Collins M F and Windsor C G 1966 *J. Appl. Phys.* **37** 1054
[4] Teaney D T, Freiser M J and Stevenson R W H 1962 *Phys. Rev. Lett.* **9** 212
[5] Freiser M J, Seiden P E and Teaney D T 1963 *Phys. Rev. Lett.* **10** 293
[6] Chaddha G and Seehra M S 1980 *Solid State Commun.* **44** 1097
[7] Heilmann I U, Kjems J K, Endoh Y, Reiter G F, Shirane G and Birgeneau R J 1981 *Phys. Rev.* B **24** 3939
[8] Teitze-Jaensch H, Sieger D, Schweiss P, Regnault L P, Jäntner H, Geick R, Treutmann W and Fåk B 1992 *J. Magn. Magn. Mater.* **104–107** 897
[9] Bruce A D and Aharony A 1975 *Phys. Rev.* B **11** 478
[10] Keffer F 1966 *Handbuch der Physik* vol 18, part 2, ed S Flugge (Berlin: Springer)
[11] Sinha K P and Kumar N 1980 *Interactions in Magnetically Ordered Solids* (Oxford: Oxford University Press)
[12] Anderson F B and Callen H B 1964 *Phys. Rev.* **136** A1068
[13] Wang Y-L and Callen H B 1964 *J. Phys. Chem. Solids* **25** 1459
[14] Low G G, Okazi A, Stevenson R W H and Tuberfield K C 1964 *J. Appl. Phys.* **35** 998
[15] Lovesey S W 1981 *Z. Phys.* B **42** 307
[16] Press W H, Flannery B P, Teukolsky S A and Vetterling W T 1986 *Numerical Recipes* (Cambridge: Cambridge University Press)
[17] Dorner B 1972 *Acta Crystallogr.* A **28** 319
[18] Cox U J, Cowley R A, Bates S and Cussens L D 1989 *J. Phys.: Condens. Matter* **1** 3031